ACCSCIENCE PUBLISHING

Materials Science in Additive Manufacturing

ORIGINAL RESEARCH ARTICLE

# Performance evaluation of artificial hip joints 3D-printed through stereolithography using dental resin reinforced with titanium dioxide nanoparticles

**Bhre Wangsa Lenggana[1]*, Rony Akbar Majid[2], Ubaidillah[2]*, and Joko Triyono[2]**

[1]Department of Mechanical Engineering, Faculty of Engineering, Universitas Jenderal Soedirman, Purwokerto, Central Java, Indonesia

[2]Department of Mechanical Engineering, Faculty of Engineering, Universitas Sebelas Maret, Surakarta, Central Java, Indonesia

## Abstract

Hip osteoarthritis is a degenerative joint disease commonly associated with aging. One effective treatment to restore patients' quality of life is total hip arthroplasty, in which the damaged hip joint is replaced with a prosthetic implant. Currently, there is a growing demand for customized artificial hip joints tailored to individual anatomical dimensions. However, the conventional casting method generally used to fabricate these implants is often considered ineffective. Additive manufacturing technology, also known as 3D printing, has emerged as a promising alternative. This technology enables the fabrication of complex designs with high accuracy and customizable geometries and sizes without altering the physical components of the 3D printing machine. This study aims to develop a 3D-printed artificial hip joint prosthesis using a dental photopolymer resin reinforced with titanium dioxide ($TiO_2$) nanoparticles. The mechanical performance of the prostheses was evaluated through both experimental and simulated compression testing. Four concentrations of $TiO_2$ nanoparticles were tested, namely 0%, 1%, 3%, and 5%. The results showed that the prosthesis reinforced with 3% $TiO_2$ nanoparticles exhibited the highest strength (717.2 N), while the one with 5% $TiO_2$ nanoparticles exhibited the lowest strength (241.8 N).

***Keywords:*** Additive manufacturing; 3D printing; Titanium oxide nanoparticles; Hip joint prosthesis; Stereolithography

***Corresponding authors:**
Bhre Wangsa Lenggana (bhre.lenggana@unsoed.ac.id)
Ubaidillah (ubaidillah_ft@staff.uns.ac.id)

**Citation:** Lenggana BW, Majid RA, Ubaidillah, Triyono J. Performance evaluation of artificial hip joints 3D-printed through stereolithography using dental resin reinforced with titanium dioxide nanoparticles. *Mater Sci Add Manuf*. 2025;4(3):025200032. doi: 10.36922/MSAM025200032

**Received:** May 14, 2025

**1st revised:** June 20, 2025

**2nd revised:** June 30, 2025

**Accepted:** June 30, 2025

**Published online:** August 1, 2025



## 1. Introduction

Osteoarthritis of the hip joint is commonly associated with aging and often results in difficulty performing activities such as walking or running. Other contributing factors include obesity and injuries to the hip joint.[1] To improve the quality of life of patients with hip osteoarthritis, total hip replacement surgery–a clinically and cost-effective procedure–is often recommended. According to a study conducted in the United States, over 300,000 patients with hip osteoarthritis undergo hip replacement surgery annually.[2]

During the procedure, the damaged joint of osteoarthritis patients is replaced with an artificial hip prosthesis, which typically consists of several components, including the acetabular cup, acetabular liner, femoral head, and femoral stem. The acetabular cup, femoral head, and femoral stem are generally fabricated from metal alloys, while the acetabular liner is composed of a polymer material.[3]

Casting is the conventional manufacturing process for artificial hip joint components such as the femoral stem and femoral head. Among the various casting methods, investment casting is widely used due to its ability to produce components in large quantities with uniform dimensions, complex geometries, and good surface finishes.[4] However, the demand for customized artificial hip joints tailored to individual patient anatomy is increasing. Conventional casting methods are considered ineffective for this purpose because customized implants require patient-specific dimensions, making casting less efficient in terms of production time and costs.[5] Additive manufacturing technology, also known as 3D printing, has emerged to fabricate parts with complex designs, diverse geometries, and varying sizes with high precision without requiring modifications to the physical hardware of the printing machine. The fundamental mechanism of this technology involves converting a 3D computer-aided design model into a physical object by sequentially arranging layers of materials.[6] There are several types of 3D printing technology, including selective laser sintering, fused deposition modeling (FDM), selective laser melting (SLM), and stereolithography (SLA).[7] SLA 3D printing uses ultraviolet light to solidify a photopolymer resin into precise, detailed objects.

Several studies have investigated the fabrication of artificial hip joint components using 3D printing technology. For instance, Wang *et al.*[3] investigated the fabrication of acetabular cup components using the SLM 3D printing method with $Ti_6Al_4V$ alloy. In a separate study, Kang *et al.*[5] fabricated acetabular cup components from titanium alloy using the PBF 3D printing method. In contrast, the current study focuses on the fabrication of femoral stem and femoral head components of artificial hip joints using the SLA 3D printing method. The material used in this study was a dental photopolymer resin reinforced with titanium dioxide ($TiO_2$) nanoparticles. Before conducting this research, the mechanical properties of the materials used in this study had been obtained for the simulation test. This research aims to evaluate the performance of the fabricated artificial hip joint prostheses through finite element analysis and experimental compression testing.

## 2. Materials and methods

### 2.1. Experimental setup and fabrication

In this study, the artificial hip joint design was created using Fusion 360 software (Autodesk, Inc., United States) based on the previous research design conducted by Ishihara.[8] Figure 1 shows the design created with the software.

The fabrication of prostheses began with the preparation of composite materials. The composite materials were prepared by mixing photopolymer resin and $TiO_2$ nanoparticles (Jiangsu Xfnano Materials Tech Co., Ltd., China). The photopolymer resin used was a dental resin-type photopolymer resin (Esun Dental Model Resin, Shenzhen Esun Industrial Co., Ltd., China). Dental resin was chosen because it is commonly used in the medical field, namely, dental care and repair by dentists.[9,10] Three variations of $TiO_2$ concentration (1%, 3%, and 5% weight) were added to the resin. The materials were measured using a digital scale (TN-Series, TN Lab, USA) with a capacity of 100 g and an accuracy of 0.001 g. The composite materials were then mixed using a magnetic stirrer (MSH-A, Daihan, South Korea) for 30 minu, followed by an ultrasonic mixer (Krisbow 10250184, Indonesia) for 90 min for all variations. The mixed $TiO_2$ nanoparticle composite material was then used for the artificial hip joint printing process using 3D printing SLA with a 3D printer (Creality Halot Sky Cl-89 SLA, Shenzhen Creality 3D Technology Co., Ltd., China). The setup parameters used were 70 s bottom exposure time, 4 s light off delay, 1 mm/s motor speed, 6 mm bottom lighting distance, and 3 s exposure time. Figure 2 shows the fabrication process of an artificial hip joint.

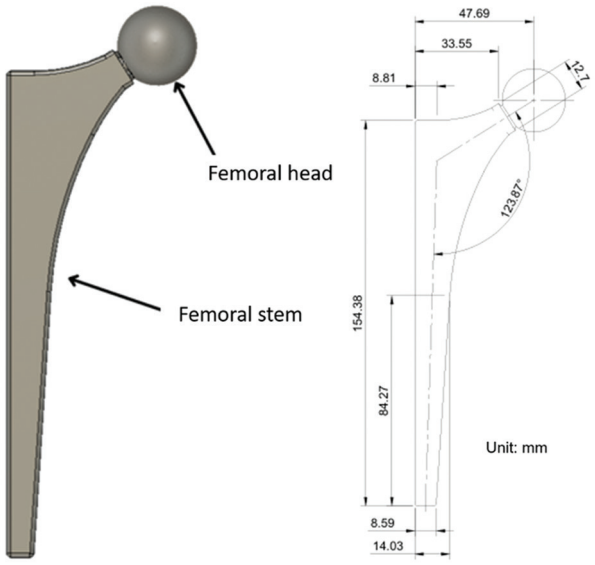


**Figure 1.** The design and dimensions of the artificial hip joint prosthesis

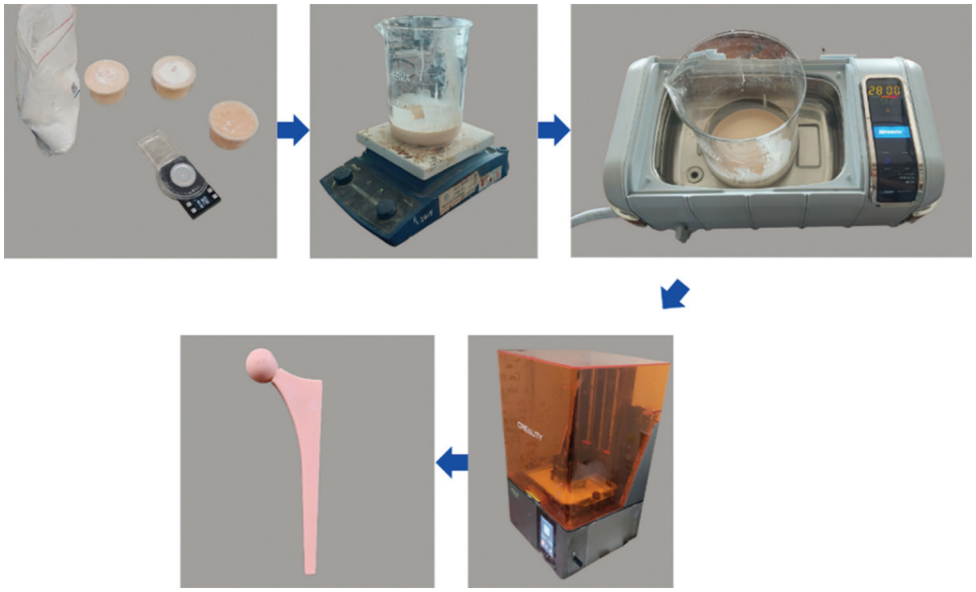

**Figure 2.** Fabrication process of an artificial hip joint

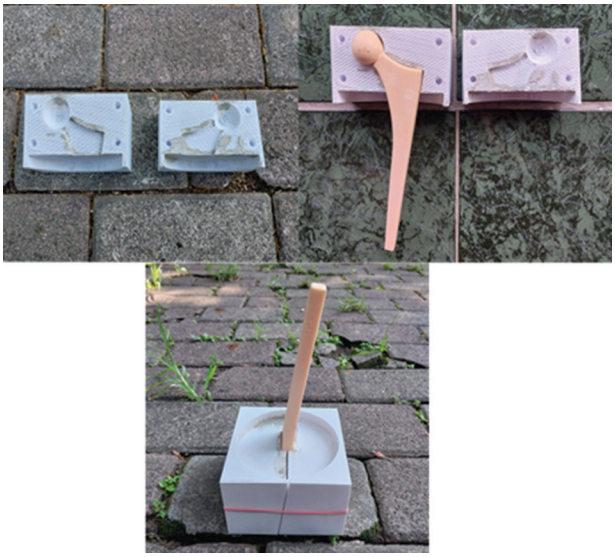

**Figure 3.** Template installation for the artificial hip joint bracket

The artificial hip joint samples were then subjected to a compression test using the universal testing machine (JTMS510, J.T.M. Technology Co., Ltd., China). The compression test was performed until the artificial hip joint was deformed or damaged. The standard used in this test was ISO 7206-6.[11] To install the artificial hip joint on the bracket according to the standard provisions, a template was created using FDM 3D printing (Figure 3). After creating the template, the next step was to lock the position of the artificial hip joint with a bracket. The bracket was constructed using a 3-inch diameter polyvinyl chloride pipe, which was then cast with a cement mixture

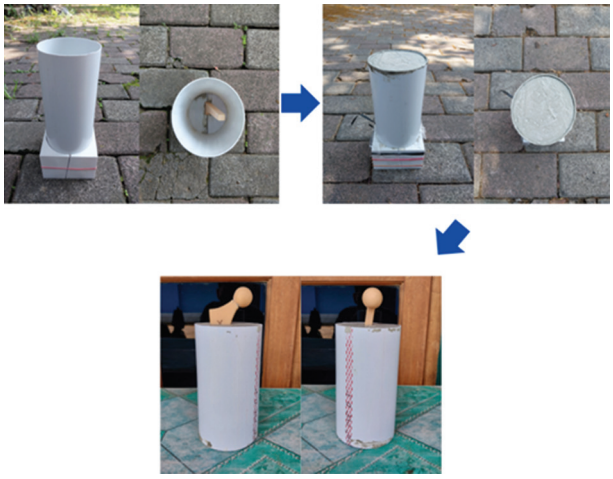

**Figure 4.** Fabrication of a bracket for the artificial hip joint compression test

(Figure 4). The compression test was then performed according to the scheme as shown in Figure 5.

## 2.2. Materials used in 3D printing

Photopolymer resins are commonly used in photopolymerization-based processes such as SLA and digital light processing. Photopolymerization involves the use of monomers or oligomers in a liquid state, along with a photoinitiator, which converts light energy into reactive species and initiates the polymerization process. The photopolymer resin was mixed with the $TiO_2$ nanoparticles–chemicals in the form of white solid granules–to strengthen the resin matrix. This material is considered technologically important due to several

properties, including ease of synthesis, good tensile strength, adequate biocompatibility, and low toxicity, as well as antibacterial and photocatalytic activity. These nanoparticles are widely used as catalyst supports in biomedicine, water and air purification, pigments, cosmetics, solar cells, and tissue engineering.[12,13] The $TiO_2$ nanoparticles used in this study were nanoparticles with an average particle diameter of 10 nm.

### 2.3. Numerical simulation

Before conducting a finite element analysis, the mechanical properties of the material were determined for simulation purposes. These properties were derived from experimental engineering stress–strain data, which were subsequently converted into actual stress–strain data and input into the finite element analysis software. The material used in the simulation was a composite consisting of dental photopolymer resin reinforced with $TiO_2$ nanoparticles. The engineering stress–strain behavior of this composite has been previously characterized. Curve fitting was performed based on the experimental engineering stress–strain graph data, and the fitting process was refined until an $R^2$ value of ≥0.95 was achieved. The resulting mechanical properties of the composites obtained from the study are shown in Table 1.

### 2.4. Sample characterization

The mechanical properties of $TiO_2$ nanoparticle composites were validated by conducting tensile test simulations using ANSYS software (Ansys, Inc., United States). The simulations were performed on specimens conforming to ASTM D638-14 type V standards. The dimensions of the specimens are shown in Figure 6. The boundary conditions applied were fixed support on side A and a velocity of 1 mm/min moving upward parallel to the Y-axis on side B (Figure 7). The tensile test simulation was set up following the experimental setup. The results of the tensile test simulation were compared with the experimental test, as shown in Figure 8. The mechanical properties of $TiO_2$ nanoparticle composites were considered valid if the difference or error between the two tests was ≤5%. This standard was also applied to the simulation process to validate consistency between the experiment and simulation. The tensile test sample was fabricated using the same 3D printing tool as the fabrication of compression test samples, as explained in the methodology section. We used a speed of 1 mm/min and provided details of the specimen dimensions in tensile testing. While in compression testing, we applied the ISO 7206-6 standard. This standard provides information on the position of the artificial hip joint placement, including both the installation depth and angle of the artificial hip joint to the bracket. The compression speed in this test was 2 mm/min.

**Table 1. Mechanical properties of dental photopolymer resin with varying concentration of $TiO_2$ nanoparticle reinforcement**

| Mechanical properties | Value | | | |
|---|---|---|---|---|
| | 0% $TiO_2$ | 1% $TiO_2$ | 3% $TiO_2$ | 5% $TiO_2$ |
| Density (g/cm3) | 1.13 | 1.15 | 1.19 | 1.20 |
| Young's modulus (MPa) | 201 | 232 | 317 | 365 |
| Poisson's ratio | 0.43 | 0.43 | 0.43 | 0.43 |
| Yield tensile strength (MPa) | 17.99 | 22.80 | 28.29 | 21.62 |
| Ultimate tensile strength (MPa) | 38.44 | 40.32 | 43.90 | 34.83 |

Abbreviation: $TiO_2$: Titanium dioxide.

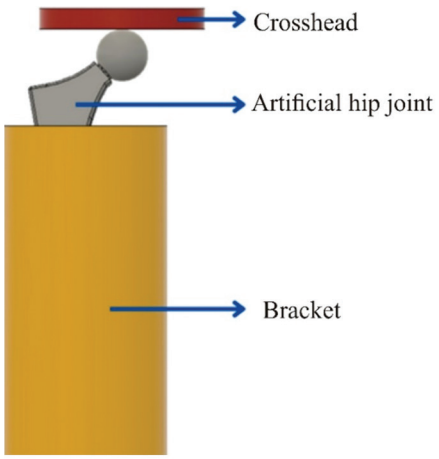


**Figure 5.** Schematic illustration of the artificial hip joint compression test

This setting was also used in the simulation process, with boundary conditions set according to the ISO standard.

A finite element study simulates the compression test to be performed on the artificial hip joint. Finite element simulation testing was performed using Ansys software based on the ISO 7206-6 test standard. This standard provides information on the placement position of the artificial hip joint, including both the depth and angle of installation of the artificial hip joint to the bracket.[11] According to the ISO 7206-6 standard, the angle of installation of the artificial hip joint must be $\alpha = 10°$ and $\beta = 9°$, with a depth of installation to the bracket as in the real case of total or partial hip joint replacement, as shown in Figure 9A.

To shorten the simulation time, the bracket geometry was excluded from the simulation process. Instead, the boundary conditions were set, namely, the femoral stem section was defined as a fixed support following the ISO 7206-6 standard. Then, the crosshead geometry that pressed the artificial hip joint was defined as moving downward in the Y-axis direction at a speed of 2 mm/min, as shown

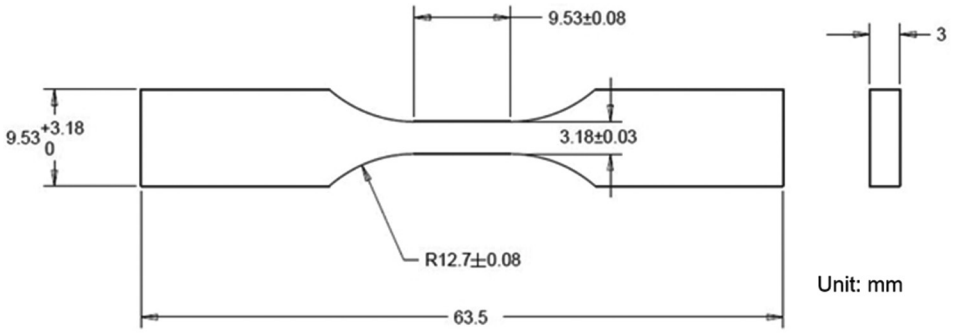


**Figure 6.** Specimen dimensions for tensile testing based on ASTM D638-14 type V standards

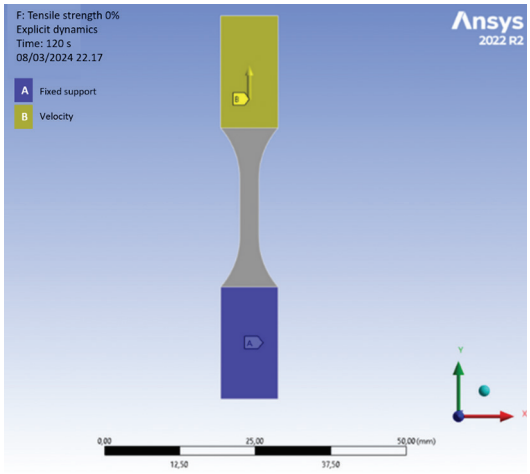


**Figure 7.** Boundary condition setup for tensile simulation

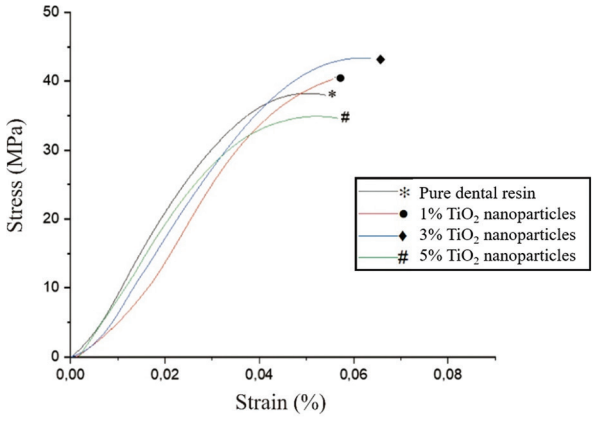


**Figure 8.** Experimental result of the tensile test

in Figure 9B. Figure 9C shows the mesh settings. For the artificial hip joint, a mesh setting with a size of 7.079 mm was applied, which went through a mesh convergence test process. For the crosshead geometry, a body sizing mesh setting with a size of 20 mm was applied. Finally, a contact sizing mesh setting was applied between the artificial hip joint geometry and the crosshead with a size of 3 mm.

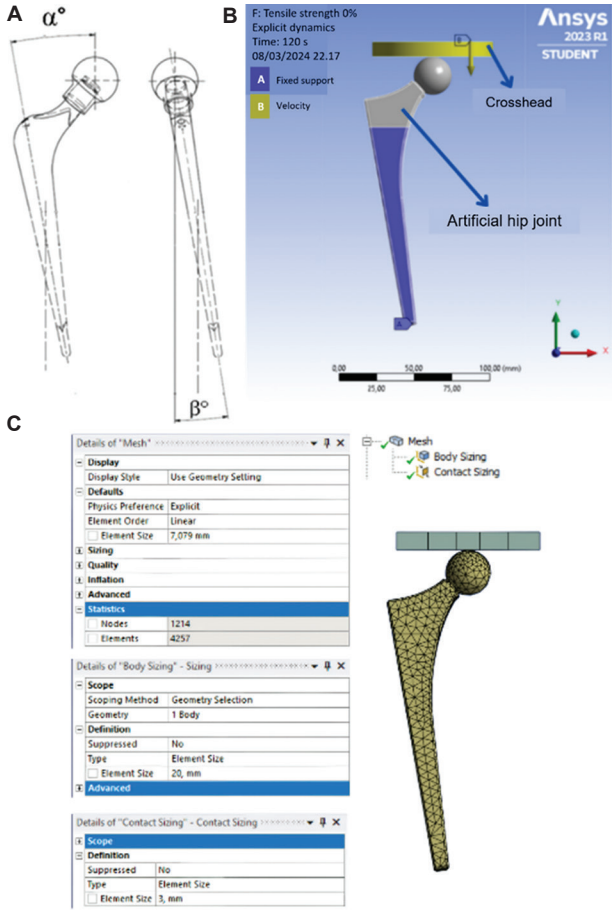


**Figure 9.** Simulation setup (A) Installation angle of artificial hip joint bracket. (B) Boundary condition setup for compression test simulation. (C) Meshing process setup for compression test simulation

## 3. Results and discussion

### 3.1. Validation of mechanical properties of $TiO_2$ nanoparticle composites

The mechanical properties of $TiO_2$ nanoparticle composites were validated by comparing the tensile strength at break values of the experimental tensile test with the

simulated tensile strength obtained using Ansys software. A threshold difference or error limit of 5% was set between the experimental and simulated tensile test results. The test results are shown in Figure 10. The average difference or error obtained at this stage was 0.96% (Table 2). The results indicate that the mechanical properties of the $TiO_2$ nanoparticle composite used to conduct the simulation were valid. The mechanical properties of the $TiO_2$ nanoparticle composite were then used to perform artificial hip joint compression test simulations.

### 3.2. Experimental results and simulation of artificial hip joint compression testing

The maximum load and displacement data of the artificial hip joint were obtained from the compression test. Maximum load data were defined as the maximum load received by the artificial hip joint before it was deformed or damaged. Displacement data were the amount of crosshead movement or deformation at maximum load on the artificial hip joint. In the experimental test, the highest maximum load and displacement values were obtained with 3% $TiO_2$, at 717.2 N and 3.56 mm, respectively. In contrast, the lowest maximum load and displacement values were obtained with 5% $TiO_2$, at 241.8 N and 2.32 mm, respectively. In the simulation test, the highest maximum load and displacement values were also obtained with 3% $TiO_2$, at 698.42 N and 4.43 mm, respectively. Similarly, the lowest maximum load and displacement values were also obtained with 5% $TiO_2$, at 241.07 N and 1.64 mm, respectively (Figures 11 and 12).

**Table 2. Comparison of experimental and simulated tensile test results**

| Tensile strength at break | Experiment (MPa) | Simulation (MPa) | Error (%) |
|---|---|---|---|
| 0% $TiO_2$ nanoparticles | 38.4 | 38 | 1.04 |
| 1% $TiO_2$ nanoparticles | 40.3 | 40.9 | 1.48 |
| 3% $TiO_2$ nanoparticles | 43.9 | 44.1 | 0.45 |
| 5% $TiO_2$ nanoparticles | 34.8 | 34.5 | 0.86 |
| Average error | | | 0.96 |

Abbreviation: $TiO_2$: Titanium dioxide.

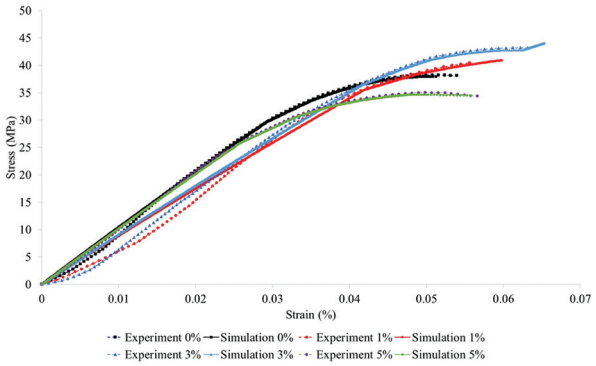


**Figure 10.** Comparison between experimental and simulated results of the tensile test

Figure 10 shows a similar trend between the experimental test graph and the simulation test graph, with only a slight difference in the curves between the two tests. Similarly, Figures 11 and 12 also displays a similar trend between the experimental test graph and the simulation test graph. However, there are remarkable differences in the results for variations in $TiO_2$ concentrations of 1%, 3%, and 5%. This may be due to the use of tensile test data for simulation, as the experimental test performed on the artificial hip joint was a compression test. This may result in differences between the experimental and simulated results of the artificial hip joint displacement. Based on the trends from Figures 11 and 12, the results of the experimental and simulated tests are acceptable.

Figure 11 shows that the addition of $TiO_2$ nanoparticles up to a concentration of 3% increased the maximum load of artificial hip joints. However, the addition of $TiO_2$

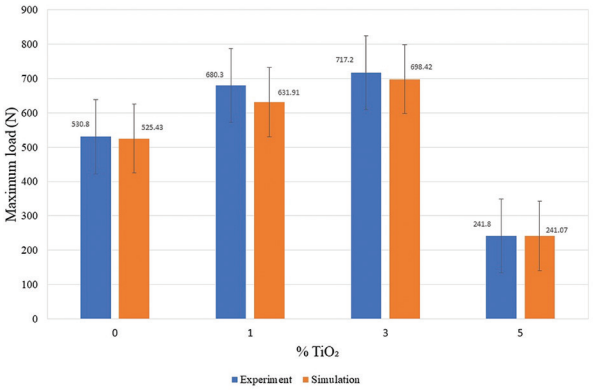


**Figure 11.** Maximum load data from experimental and simulated results

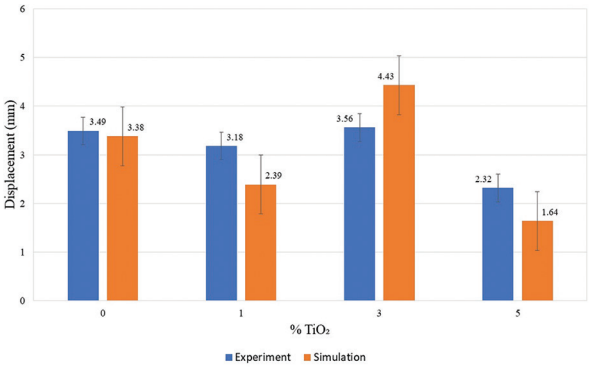


**Figure 12.** Displacement data from experimental and simulated results

nanoparticles beyond 3% reduces the maximum load of artificial hip joints. A similar phenomenon is found in the tensile test results. The initial increase in strength is attributed to enhanced intermolecular interactions. $TiO_2$ nanoparticles possess a high surface area-to-volume ratio, and when uniformly dispersed within the resin matrix, they significantly increase the surface area available for bonding. This promotes stronger interactions between the nanoparticles and the surrounding resin, improving internal adhesion and ultimately enhancing the mechanical strength of the composite material. In addition, the increase in strength is also attributed to the nanoscale reinforcement. Nanoparticles are effective reinforcing materials that can interact with polymer chains in the resin, restricting their mobility and thereby increasing stiffness and resistance to deformation of the overall structure. This interaction significantly enhances the stiffness, tensile strength, and compressive strength of the resulting composite material.[14] However, when the concentration of $TiO_2$ nanoparticles exceeds a certain threshold, agglomeration may occur. The formation of nanoparticle clusters disrupts the uniform dispersion within the resin matrix, leading to stress concentrations and weakened interfacial bonding.[15] As a result, the mechanical strength of the dental photopolymer resin composite may decrease.

Figure 13 compares the behavior of the artificial hip joint prosthesis between the experimental and simulated compression tests. The figure shows similar behavior of the artificial hip joint prosthesis between the experimental and the simulated compression test, with only a slight difference in the fracture shape when the artificial hip joint prosthesis breaks.

### 3.3. Micrograph analysis

The results of scanning electron microscopy (SEM) indicate that the fracture surface of the specimen is smooth and neat in pure photopolymer as shown in Figure 14A. After the addition of nanoparticles, the specimen surface looks rougher. In Figure 14B-D, there are clumps indicated by arrows; the larger the $TiO_2$ nanoparticles used, the more clumping and voids appear. Roughness on the fracture surface indicates an increase in the mechanical strength of the specimen. When combining SLA resin with $TiO_2$ nanoparticles, several characteristic features are expected from the SEM images. SEM imaging provides detailed surface information, revealing the distribution, morphology, and interaction of nanoparticles within the resin matrix. A uniform dispersion of $TiO_2$ nanoparticles throughout the resin matrix should be observed in the SEM images, indicating a uniform dispersion and successful incorporation of the nanoparticles into the resin. This uniform dispersion signifies good interaction between the nanoparticles and the resin, which is crucial for enhancing the mechanical strength of the composite.

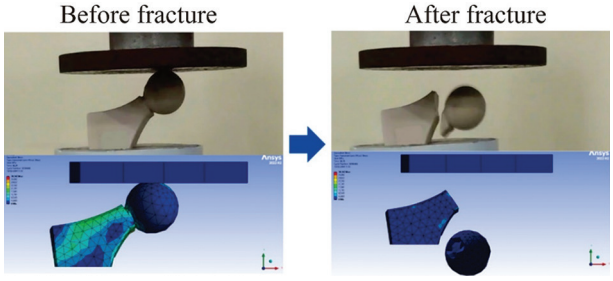


**Figure 13.** In-frame comparison of the experiment with simulation

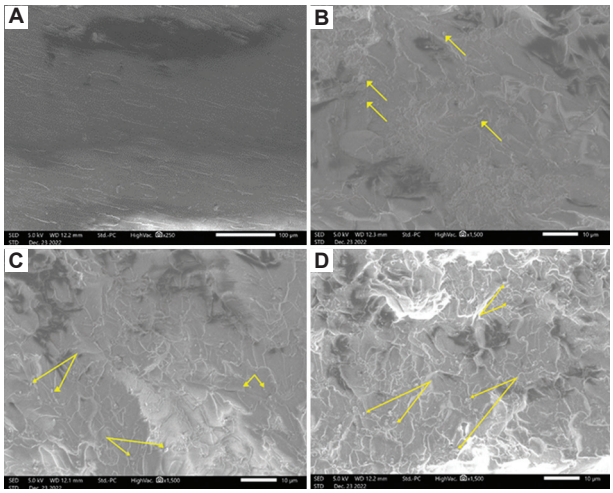


**Figure 14.** Scanning electron microscopy images of the fracture surface. (A) Pure resin at ×250 magnification with 100 µm scale bar. (B) 1% weight $TiO_2$ at ×1,500 magnification with 10 µm scale bar. (C) 3% weight $TiO_2$ at ×1,500 × magnification with 10 µm scale bar. (D) 5% weight $TiO_2$ at ×1,500 magnification with 10 µm scale bar

Individual $TiO_2$ nanoparticles should be visible as distinct entities in the SEM images, indicating proper dispersion with minimal agglomeration. The presence of individual nanoparticles contributes to strengthening the composite and enhancing various functional properties. Although small aggregates of $TiO_2$ nanoparticles form when nanoparticles come into proximity and may be present in the SEM images, these aggregates do not form large clusters or lumps. These aggregates offer improved mechanical and functional properties comparable to individual nanoparticles. Besides, an adequate surface coverage of $TiO_2$ nanoparticles on the resin matrix should also be observed in the SEM images. The nanoparticles should be evenly distributed across the resin's surface, creating a continuous or semi-continuous layer. This surface coverage ensures effective reinforcement and desired functional properties, such as increased strength, improved thermal stability, or enhanced optical properties.

In addition to nanoparticle distribution, SEM images can also reveal the morphological characteristics of the $TiO_2$ nanoparticles. The nanoparticles may exhibit various shapes, such as spherical, rod-like, or irregular structures, depending on their synthesis method and properties. Observing the morphology of the nanoparticles provides insights into their behavior and interaction within the resin matrix.

The presence of lumps in SEM images of SLA resin reinforced with $TiO_2$ nanoparticles can be attributed to several factors, including the resin composition, nanoparticle dispersion, processing conditions, and sample preparation. One of the primary causes of lump formation is the agglomeration of nanoparticles. During the fabrication process, $TiO_2$ nanoparticles may agglomerate due to interparticle forces such as van der Waals forces or electrostatic interactions, resulting in the formation of larger clusters or lumps. Additionally, inadequate dispersion of nanoparticles within the resin matrix can also contribute to the formation of lumps. Therefore, a homogeneous distribution of nanoparticles is crucial. Factors such as insufficient mixing, improper choice of dispersants, or high viscosity of the resin can restrict the effective dispersion of nanoparticles. Moreover, the curing or drying process of the SLA resin can also contribute to the formation of lumps. As SLA resins undergo a curing or drying process to solidify the material, the resin may not solidify uniformly if the curing conditions, such as temperature or curing time, are not properly controlled. This non-uniform solidification can result in the formation of lumps or irregularities on the resin's surface. Sample preparation for SEM analysis is another critical aspect to consider. Improper sample preparation can introduce artifacts or contaminants that appear as lumps in the SEM images. For example, incomplete cleaning or inadequate drying of the sample can leave residues or moisture that form irregularities or lumps in the images. To address the issue of lump formation, several strategies can be employed. Optimizing the dispersion process during resin formulation or fabrication can help prevent agglomeration and ensure a uniform distribution of nanoparticles. Controlling the curing or drying conditions is also important in achieving consistent solidification of the resin. Finally, proper sample cleaning and drying techniques should be employed to minimize the introduction of artifacts during the SEM sample preparation.

### 3.4. Benchmarking

Da Costa *et al.*[11] conducted a study on the fabrication of artificial hip joints using polyurethane reinforced with glass fiber. The fabricated prosthesis has a modulus of elasticity comparable to the human femur. The strength test results based on the ISO 7206-6 standard of the fabricated prosthesis are shown in Table 3. Three variations of composites were utilized to fabricate the prosthesis in the study, namely polyurethane, polyurethane with 16 strands of glass fiber reinforcement, and a mixture of polyurethane and calcium carbonate with 16 strands of glass fiber reinforcement (PUCa16G). Of the three variations, the PUCa16G variation results in the highest maximum load of 1,739.73 N. In addition, the PUCa16G variation has a modulus of elasticity similar to the human femur.[11]

Figure 15 shows the comparison of compression test results between the study by Da Costa *et al.*[11] and the present study. It can be seen that the strength of the artificial hip joint fabricated with $TiO_2$ nanoparticle composite is significantly lower than PUCa16G composite. This is mainly due to the difference in the reinforcing materials used, where two reinforcing materials, calcium carbonate and glass fiber, were utilized by Da Costa *et al.*[11] In addition, the maximum load of the artificial hip joint fabricated with $TiO_2$ nanoparticle composite is also remarkably low compared to the one fabricated using PUCa16G composite, as the strength of the dental photopolymer resin matrix is weaker than the polyurethane matrix. The results of the

**Table 3. Result from the study by Da Costa *et al.*,[11] based on ISO 7206-6**

| Materials | Maximum load (N) | Displacement (mm) |
|---|---|---|
| PU | 911.90±82.01 | 4.67±0.71 |
| PU16G | 1043.84±132.57 | 8.34±1.56 |
| PUCa16G | 1739.73±79.68 | 5.07±1.12 |
| Nanoparticle $TiO_2$ | 717.2 | 3.56 |

Abbreviations: PU: Polyurethane; PU16G: Polyurethane with 16 strands of glass fiber reinforcement; PUCa16G: A mixture of polyurethane and calcium carbonate with 16 strands of glass fiber reinforcement.

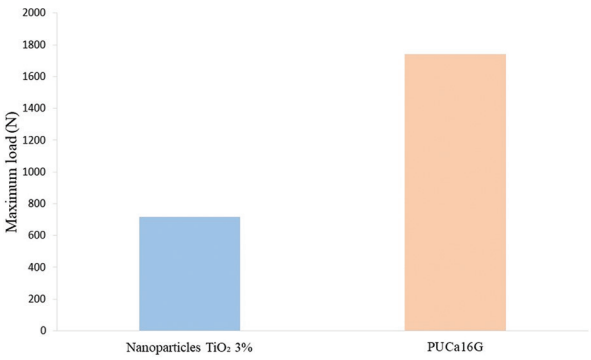


**Figure 15.** Comparison of the maximum load of the artificial hip joints between Da Costa *et al.*[11] and the present study
Abbreviation: PUCa16G: A mixture of polyurethane and calcium carbonate with 16 strands of glass fiber reinforcement

present study are not comparable to the study of Da Costa *et al.*[11] due to the significant difference in material strength. These results were compared because the same prototypes were fabricated, both of which were artificial hip joint prosthesis prototypes. Despite the significant difference in the strength of the artificial hip joint prosthesis, the fabrication of prostheses using the 3D printing or additive manufacturing method is still promising for further research considering the advantages of this method, such as being able to fabricate complex designs with high accuracy and customizable geometries without altering the physical components to the 3D printing machine.

## 4. Conclusion

The performance of artificial hip joint prosthesis fabricated using dental photopolymer resin reinforced with varying concentration (0%, 1%, 3%, and 5% weight) of $TiO_2$ nanoparticles using a 3D printing method was investigated. A simulated compression test of the artificial hip joint has been conducted, which shows that the 3% $TiO_2$ exhibits the highest maximum load value among all variations. This is in accordance with the experimental compression testing performed in this study. In contrast, the lowest values are reported at 5% weight $TiO_2$. Based on the analysis conducted, the simulation results closely correspond to the experimental results. However, the performance of the hip joint prosthesis fabricated in the present study is weaker compared to previous research utilizing stronger materials. Despite the limitation in performance, the SLA 3D printing method remains a viable approach for further research due to its ability to fabricate a wide range of prostheses without requiring modifications to the 3D printer.

## Acknowledgments

We would like to acknowledge the Universitas Sebelas Maret for providing the materials/equipments/etc., for this study.

## Funding

This research was supported by the Laboratory of Vibration and Additive Manufacturing of Universitas Sebelas Maret.

## Conflict of interest

The authors declare no competing interests.

## Author contributions

*Conceptualization:* Ubaidillah, Joko Triyono
*Formal analysis:* Ubaidillah, Joko Triyono
*Investigation:* Bhre Wangsa Lenggana, Rony Akbar Majid
*Methodology:* Rony Akbar Majid, Bhre Wangsa Lenggana, Ubaidillah
*Writing – original draft:* Bhre Wangsa Lenggana
*Writing – review & editing:* Bhre Wangsa Lenggana, Rony Akbar Majid

## Ethics approval and consent to participate

Not applicable.

## Consent for publication

Not applicable.

## Availability of data

No datasets were generated or analyzed during the current study.

## References

1. Gross JB, Guillaume C, Gégout-Pottie P, Mainard D, Presle N. Synovial fluid levels of adipokines in osteoarthritis: Association with local factors of inflammation and cartilage maintenance. *Biomed Mater Eng*. 2014;24(S1):17-25.

   doi: 10.3233/bme-140970

2. Kurtz SM, Ong KL, Lau E, Bozic KJ. Impact of the economic downturn on total joint replacement demand in the United States. *J Bone Joint Surg*. 2014;96(8):624-630.

   doi: 10.2106/jbjs.m.00285

3. Wang C, Sun B, Zhang Y, Wang C, Yang G. Design of a novel trabecular acetabular cup and selective laser melting fabrication. *Materials*. 2022;15(17):6142.

   doi: 10.3390/ma15176142

4. Ismail R, Bayuseno AP, Fitriyana DF, *et al*. Mechanical properties characterization of Ti6Al4V for artificial hip joint materials prepared by investment casting. *IOP Conf Ser Earth Environ Sci*. 2022;969(1):012001.

   doi: 10.1088/1755-1315/969/1/012001

5. Kang Y, Sun DH, Park JC, Kim J. Shape suitability and mechanical safety of customised hip implants: Three-dimensional printed acetabular cup for hip arthroplasty. *J Orthop*. 2022;34:166-172.

   doi: 10.1016/j.jor.2022.08.011

6. Guo N, Leu MC. Additive manufacturing: technology, applications and research needs. *Front Mech Eng*. 2013;8(3):215-243.

   doi: 10.1007/s11465-013-0248-8

7. Grygier D, Kujawa M, Kowalewski P. Deposition of biocompatible polymers by 3D printing (FDM) on titanium alloy. *Polymers*. 2022;14(2):235.

   doi: 10.3390/polym14020235

8. Ishihara K. Highly lubricated polymer interfaces for advanced artificial hip joints through biomimetic design.

*Polym J*. 2015;47(9):585-597.

doi: 10.1038/pj.2015.45

9. Liqcreate. *Digital Dentistry and Dental Resin 3D-Printing*. Available from: https://www.liqcreate.com/supportarticles/digital-dentistry-and-dental-resin-3d-printing [Last accessed on 2023 Aug 04].
10. Esun. *Dental Resin*. Available from: https://www.esun3d.com/dental-resin/?gad_source=1&gclid=cj0kcqjwxeyxbhc7arisac7ds38iy-mpxesejk3hae1sh_yjox-m6bjfpr3ecyc6-kqwdopvify0k1oaao7_ealw_wcb [Last accessed on 2024 May 21].
11. Da Costa RR, De Almeida FR, Da Silva AA, Domiciano SM, Vieira AF. Design of a polymeric composite material femoral stem for hip joint implant. *Polímeros*. 2019;29(4):354.

    doi: 10.1590/0104-1428.02119
12. Alrahlah A, Khan R, Vohra F, *et al*. Influence of the physical inclusion of ZRO2/TIO2 nanoparticles on physical, mechanical, and morphological characteristics of PMMA-Based interim restorative material. *Biomed Res Int*. 2022;2022:1743019.

    doi: 10.1155/2022/1743019
13. Bukichev YS, Bogdanova LM, Lesnichaya VA, Chukanov NV, Golubeva ND, Dzhardimalieva GI. Mechanical and thermophysical properties of epoxy nanocomposites with titanium dioxide nanoparticles. *Appl Sci*. 2023;13(7):4488.

    doi: 10.3390/app13074488
14. Sun J, Watson SS, Allsopp DA, Stanley D, Skrtic D. Tuning photo-catalytic activities of TiO2 nanoparticles using dimethacrylate resins. *Dent Mater*. 2016;32(3):363-372.

    doi: 10.1016/j.dental.2015.11.021
15. Hada T, Kanazawa M, Miyamoto N, *et al*. Effect of different filler contents and printing directions on the mechanical properties for photopolymer resins. *Int J Mol Sci*. 2022;23(4):2296.

    doi: 10.3390/ijms23042296